Journal of Virology®

VIRUS-CELL INTERACTIONS

The Amino Acid at Position 8 of the Proteolytic Cleavage Site of the Mumps Virus Fusion Protein Affects Viral Proteolysis and Fusogenicity

Sarah Hüttl,[a,b] Markus Hoffmann,[c,d] Torsten Steinmetzer,[e] Christian Sauder,[f] Nadine Krüger[a,b,c]

[a]Institute of Virology, University of Veterinary Medicine Hannover, Hannover, Germany
[b]Research Center for Emerging Infections and Zoonoses, University of Veterinary Medicine Hannover, Hannover, Germany
[c]Infection Biology Unit, German Primate Center, Leibniz Institute for Primate Research, Göttingen, Germany
[d]Faculty of Biology and Psychology, Georg August University Göttingen, Göttingen, Germany
[e]Institute of Pharmaceutical Chemistry, Philipps University Marburg, Marburg, Germany
[f]Food and Drug Administration (FDA), Center for Biologics Evaluation and Research (CBER), Silver Spring, Maryland, USA

ABSTRACT The mumps virus (MuV) fusion protein (F) plays a crucial role for the entry process and spread of infection by mediating fusion between viral and cellular membranes as well as between infected and neighboring cells, respectively. The fusogenicity of MuV differs depending on the strain and might correlate with the virulence; however, it is unclear which mechanisms contribute to the differentiated fusogenicity. The cleavage motif of MuV F is highly conserved among all strains, except the amino acid residue at position 8 (P8) that shows a certain variability with a total of four amino acid variants (leucine [L], proline [P], serine [S], and threonine [T]). We demonstrate that P8 affects the proteolytic processing and the fusogenicity of MuV F. The presence of L or S at P8 resulted in a slower proteolysis of MuV F by furin and a reduced ability to mediate cell-cell fusion. However, virus-cell fusion was more efficient for F proteins harboring L or S at P8, suggesting that P8 contributes to the mechanism of viral spread: P and T enable a rapid spread of infection by cell-to-cell fusion, whereas viruses harboring L or S at P8 spread preferentially by the release of infectious viral particles. Our study provides novel insights into the fusogenicity of MuV and its influence on the mechanisms of virus spread within infected tissues. Assuming a correlation between MuV fusogenicity and virulence, sequence information on the amino acid residue at P8 might be helpful to estimate the virulence of circulating and emerging strains.

IMPORTANCE Mumps virus (MuV) is the causative agent of the highly infectious disease mumps. Mumps is mainly associated with mild symptoms, but severe complications such as encephalitis, meningitis, or orchitis can also occur. There is evidence that the virulence of different MuV strains and variants might correlate with the ability of the fusion protein (F) to mediate cell-to-cell fusion. However, the relation between virulence and fusogenicity or the mechanisms responsible for the varied fusogenicity of different MuV strains are incompletely understood. Here, we focused on the amino acid residue at position 8 (P8) of the proteolytic cleavage site of MuV F, because this amino acid residue shows a striking variability depending on the genotype of MuV. The P8 residue has a significant effect on the proteolytic processing and fusogenicity of MuV F and might thereby determine the route of viral spread within infected tissues.

KEYWORDS fusion, mumps virus, viral entry

Mumps virus (MuV) belongs to the genus *Orthorubulavirus* within the family *Paramyxoviridae*. Infection with MuV leads to the highly contagious disease mumps that is generally associated with mild symptoms such as fever or headache as

Citation Hüttl S, Hoffmann M, Steinmetzer T, Sauder C, Krüger N. 2020. The amino acid at position 8 of the proteolytic cleavage site of the mumps virus fusion protein affects viral proteolysis and fusogenicity. J Virol 94:e01732-20. https://doi.org/10.1128/JVI.01732-20.

Editor Rebecca Ellis Dutch, University of Kentucky College of Medicine

Address correspondence to Nadine Krüger, nkrueger@dpz.eu.

Received 1 September 2020
Accepted 2 September 2020
Accepted manuscript posted online 9 September 2020
Published 27 October 2020

well as the characteristic uni- or bilateral parotitis; however, more severe complications such as encephalitis, meningitis, or orchitis may occur (1–3).

MuVs are enveloped viruses with a nonsegmented, single-stranded negative-sensed RNA genome that encodes seven structural and two nonstructural proteins (4, 5). The viral entry process of MuVs comprises two steps: (i) the attachment of viruses to target cells by the binding of the viral surface glycoprotein hemagglutinin-neuraminidase (HN) to sialic acids present on cell surface macromolecules and (ii) the fusion between viral and host cell membrane, enabling the release of the viral RNA genome into the cytoplasm (6–8). Viral fusion is mediated by the fusion protein (F) that is expressed within the envelope of virus particles. Besides mediating the fusion between cellular and viral membranes, F induces the fusion between infected and neighboring cells, resulting in the formation of multinucleated giant cells, so called syncytia, to enable a rapid cell-to-cell virus spread (9, 10). MuV F is synthesized as the inactive nonfusogenic precursor protein F_0 that has to be cleaved by host cell proteases resulting in the fusogenic disulfide-linked F_1 and F_2 subunits (11). The multibasic cleavage motif R-H-K-R ↓ F-A is highly conserved among all MuV strains and is most likely cleaved by cellular furin (12), a subtilisin-like proprotein convertase mainly localized in the *trans*-Golgi network (13–15). Recently, it has been proposed that not only the multibasic cleavage motif but a total of 20 amino acid (aa) residues (P14 to P6′) comprising a core region (P6 to P2′) that fits into the catalytic pocket of furin as well as two flanking solvent accessible regions (P14 to P7 and P3′ to P6′) play an important role for the accessibility of the proteolytic cleavage motif to the cellular protease furin (16, 17). In addition to proteolytic activation, MuV F has to undergo conformational changes that are induced by the interaction between MuV F and HN to expose the hydrophobic fusion peptide present at the N terminus of the F_1 subunit toward the host cell membrane (18); consequently, the expression of both surface glycoproteins is required for viral fusion (19).

The ability to induce cell-to-cell fusion varies depending on the MuV strain. Furthermore, it has been suggested that this fusogenicity might correlate with the virulence, as most of the virulent strains show a strong fusion activity, whereas avirulent strains show a reduced or no ability to induce syncytium formation (9, 10, 20–22). So far, it is unclear why some MuV strains are highly fusion active whereas others are not. Moreover, the mechanisms that contribute to the varied fusogenicity are not known. It has been suggested that the cell-to-cell fusogenicity might negatively correlate with the neuraminidase activity of the HN protein (20); furthermore, 3 aa residues (A91, S195, and L383) within the F protein that modify the fusion activity have been identified (23–26). However, these observations were obtained for particular MuV strains, and it is not known whether they represent general features of MuV F fusogenicity that apply to all MuV strains and variants.

Here, we focused on the core region (P6 to P2′; amino acid residues 97 to 104 of F) and the flanking solvent accessible regions (P14 to P7; amino acid residues 89 to 96 of F; P3′ to P6′; amino acid residues 105 to 108 of F) of the proteolytic cleavage motif of MuV F. The entire motif is well conserved among all known MuV strains, with the exception of the amino acid residue at position 8 (P8; amino acid residue 95 of F), where either leucine (L), proline (P), serine (S), or threonine (T) are present. By the generation and characterization of peptides, F proteins and recombinant MuVs in which the amino acid residue at P8 has been modified, we were able to show that P8 has an effect on the efficiency of the proteolytic cleavage of MuV F by the host cell protease furin and modifies the fusogenicity of MuV F. Depending on the amino acid residue present at P8, two different mechanisms of virus spread within infected cell layers have been observed: (i) spread by cell-to-cell fusion between infected and neighboring cells and (ii) spread by the release of viral particles from infected cells followed by fusion between viral and cellular membranes.

Our observations provide novel insights into the differential fusogenicity of MuV and might be useful for further studies focusing on the estimation of MuV virulence. Studies aiming to identify virulence markers of MuV are very complex and might

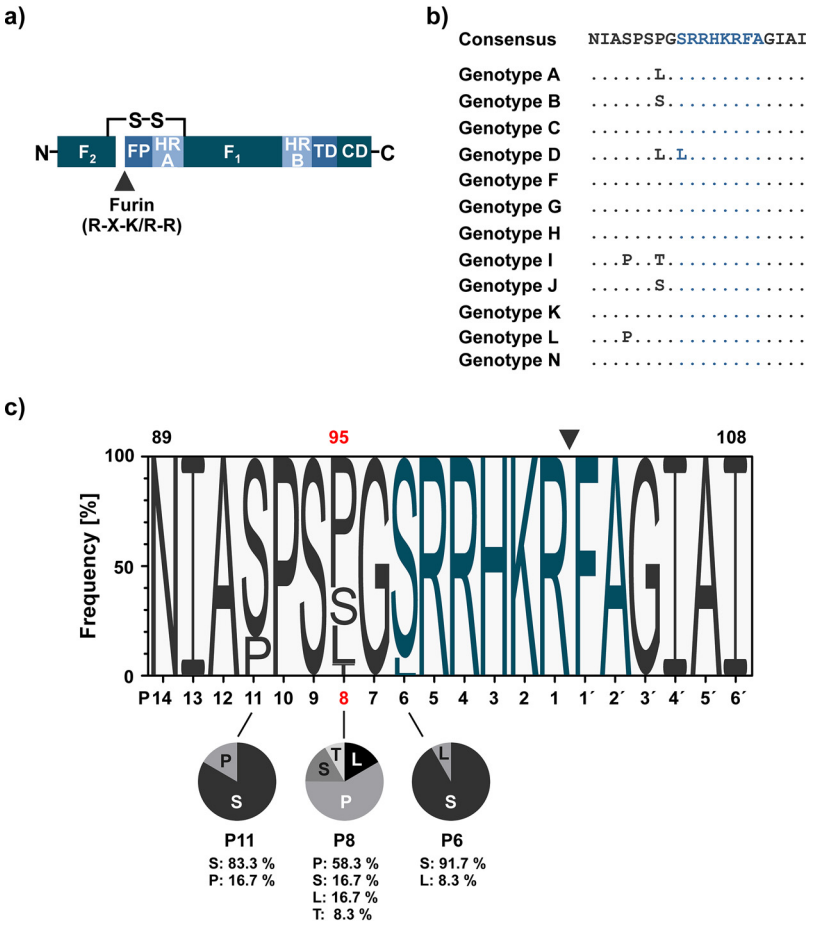

FIG 1 Homology of the proteolytic cleavage site of MuV F. (a) Schematic illustration of MuV F. F_1, F_2, $F_1/_2$ subunit; FP, fusion peptide; HRA, HRB, heptad repeat region A/B; TD, transmembrane domain; CD, cytoplasmic domain. (b) Genotype-dependent consensus sequences of P14 to P6′ residues of MuV F. (c) Frequencies of amino acid residues comprising P14 to P6′ of the proteolytic activation site based on the genotype-dependent consensus sequences. Top numbers indicate the amino acid residue of MuV F. Arrowheads indicate the proteolytic cleavage site.

include additional genes besides F. However, assuming a correlation between MuV fusogenicity and virulence, the amino acid residue at P8 should be taken into account when evaluating the virulence of circulating and emerging strains.

(Part of this work was performed by S. Hüttl in partial fulfillment of the requirements for a doctoral degree from the University of Veterinary Medicine Hannover, Germany.)

RESULTS

The amino acid residue at P8 of the furin motif varies depending on the MuV genotype. The proteolytic cleavage of MuV F occurs directly upstream of the fusion peptide at the N-terminal end of the F_1 subunit (Fig. 1a). Whereas the core of the furin motif (P6 to P2′) and the flanking solvent-accessible region downstream of the cleavage site (P3′ to P6′) share a very high homology, the amino acid identity upstream of the core region (P14 to P7) is less conserved (Fig. 1b; see also Data Set S1 in the supplemental material). Especially, the amino acid residue at P8 (amino acid residue 95 of the F protein) shows a striking variability depending on the MuV strain and seems to correlate with the genotypes of MuV as strains belonging to the same genotype—based on the nucleotide sequence of the small hydrophobic proteins—harbor the identical amino acid residue at P8 (Fig. 1b). A total of four different aa residues can be observed for this position: P is present in the majority of the MuV strains (58.3%), whereas a lower percentage of MuV strains harbors S (16.7%), L (16.7%), or T (8.3%) at the respective position (Fig. 1c).

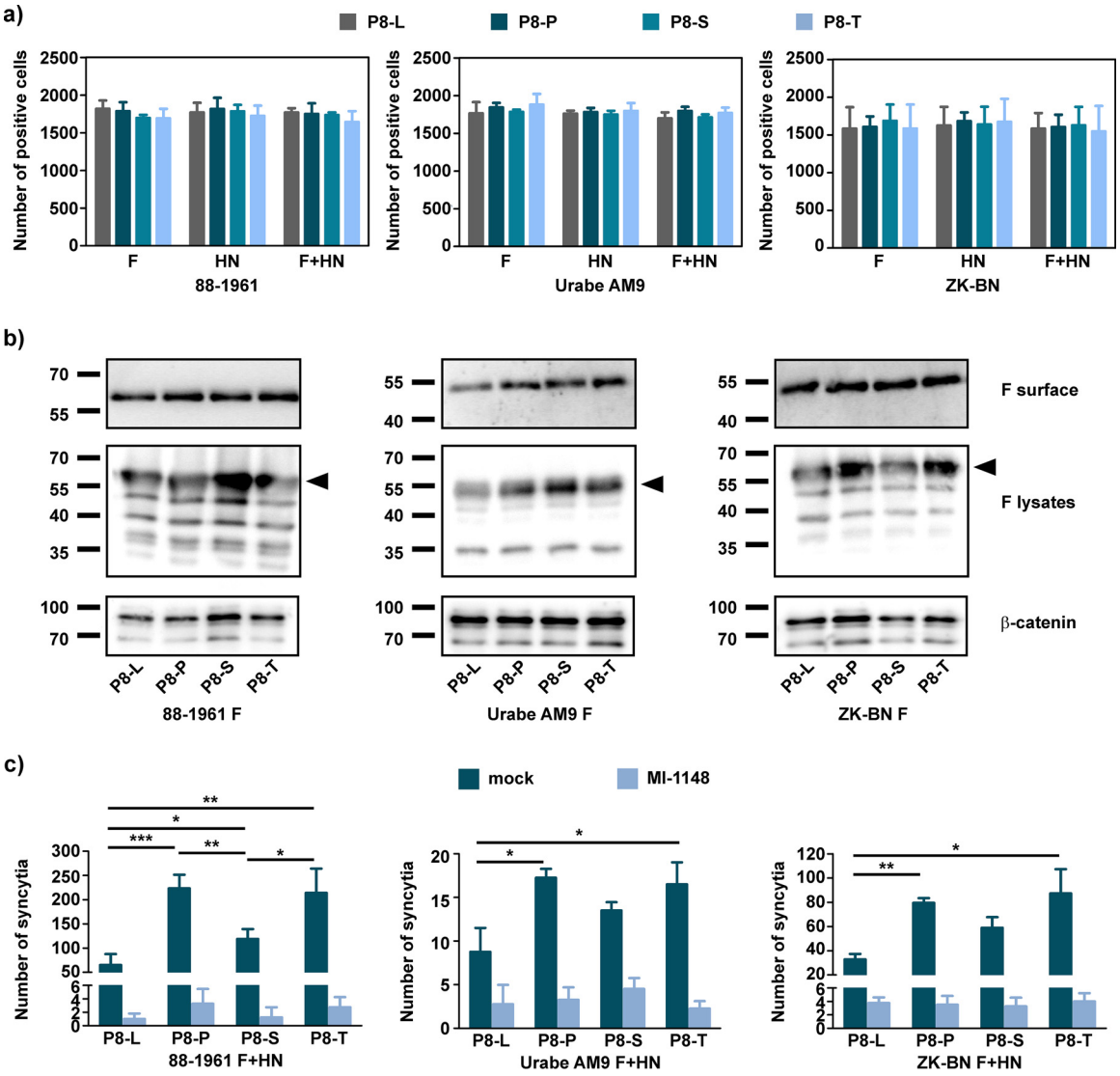

FIG 2 MuV F-induced cell-to-cell fusion depending on the amino acid residue at P8. Vero76 cells were transfected for the coexpression of 88-1961, Urabe AM9, and ZK-BN MuV F (P8-L/P/S/T) and HN. At 2 dpt, cells were fixed, and MuV F and HN were visualized by incubation with antibodies directed against the HA (F) and FLAG (HN) epitopes and fluorochrome-labeled secondary antibodies. (a) The total numbers of F-, HN-, and coexpressing cells were counted and are shown as means and standard deviations (SDs) from two independent experiments. (b) Total and surface expression levels of MuV F were investigated by SDS-PAGE and Western blotting under reducing conditions. F proteins were detected by incubation with antibodies directed against the HA epitope; β-catenin served as a loading control. Arrow heads indicate F_1. Molecular mass (kDa) is indicated on the left. Exposure times: β-catenin, 10 s; MuV F (total), 1 s; 88-1961 F (surface), 10 s; Urabe AM9 F (surface), 45 s; ZK-BN F (surface), 45 s. (c) The total numbers of syncytia per coverslip were counted. Syncytia were defined as multinucleated cells that harbored at least three nuclei and showed a positive fluorescence signal for the expression of both MuV F and HN. The graphs show means and SDs from four independent experiments. Statistical significance between the modified F proteins of each strain was tested for mock-treated cells by paired, two-tailed Student's *t* test with 95% confidence intervals. *, $P \leq 0.05$; **, $P \leq 0.01$; ***, $P \leq 0.005$.

The ability of MuV F to induce cell-to-cell fusion depends on the amino acid residue at P8. The fusogenicity of the F protein of three MuV strains (88-1961, ZK-BN, and Urabe AM9) has been analyzed by determining the formation of syncytia following coexpression of F and HN derived from the same strains. The F proteins of the highly neurovirulent strain 88-1961 (genotype H) and the ZK-BN strain (unknown genotype) that has been isolated from a hospitalized patient (27) harbor a P at P8, while the vaccine strain Urabe AM9 (genotype B) has an S instead.

The numbers of F-, HN-, and coexpressing cells were comparable for each strain regardless of the amino acid residue present at P8 (Fig. 2a). Furthermore, no differences were obtained regarding total and surface expression levels of MuV F, as well as MuV

TABLE 1 Syncytium formation in Vero76 cells following coexpression of MuV F and HN[a]

F protein	No. of syncytia	No. of nuclei per syncytium	Total no. of nuclei in fusion
88-1961 F P8-L	65.3	4.1	269.3
88-1961 F P8-P	223.3	5.1	1149.0
88-1961 F P8-S	119.0	4.4	520.0
88-1961 F P8-T	214.0	5.0	1085.3
Urabe AM9 F P8-L	8.8	3.3	28.8
Urabe AM9 F P8-P	17.3	3.5	60.3
Urabe AM9 F P8-S	13.5	4.5	60.0
Urabe AM9 F P8-T	16.5	3.5	57.6
ZK-BN F P8-L	32.8	3.7	122.5
ZK-BN F P8-P	79.5	4.4	350.0
ZK-BN F P8-S	59.0	3.8	225.8
ZK-BN F P8-T	75.8	4.0	348.75

[a]The values are means from three independent experiments.

F cleavability (Fig. 2b). For each strain, the intensities of protein bands were similar for all four F variants. All F proteins were detected as their cleaved F_1 subunit, the size of which ranged from approximately 60 to 55 kDa, probably due to differences in their glycosylation status. Besides the cleaved F_1 subunit, additional protein bands that ranged between approximately 55 and 35 kDa and might either represent premature products of F or fragments resulting from unspecific degradation were detected in cell lysates but not for F expressed on the cell surface (Fig. 2b).

As expected, the fusogenicity differed among the strains analyzed: the highest number of syncytia was obtained for 88-1961, whereas Urabe AM9 F showed the lowest fusogenicity (Fig. 2c). Regardless of the strain-specific differences in the manifestation of syncytia, a similar pattern was obtained for all three strains analyzed, The expression of L at P8 led to a significantly reduced number of syncytia; in contrast to this, the highest numbers and sizes of syncytia were obtained for F proteins harboring either P or T at P8 (Table 1). The inhibition of the cellular protease furin by the inhibitor MI-1148 reduced the ability of all F proteins to mediate cell-to-cell fusion to similar degrees, suggesting that the amino acid residue at P8 affects the fusogenicity of MuV F but not its dependence on proteolytic activation by furin (Fig. 2c).

Proteolytic cleavage by furin is more efficient for peptides harboring P or T at P8. After having shown that the fusogenicity is affected by the amino acid residue at P8, we analyzed whether the kinetics of F proteolysis vary depending on P8. Peptides consisting of the donor-quencher pair Edans/Dabcyl and the amino acid residues corresponding to P8 to P1′ of the MuV F cleavage site (Fig. 3a) were incubated with 10 nM recombinant furin. The cleavage of peptides harboring L or S at P8 occurred slower than that of peptides harboring P and T at P8, as indicated by a lower slope of their progress curves (Fig. 3b). For all peptides, maximal relative fluorescence unit (RFU) values were determined after approximately 60 min. Prolonged incubation periods resulted in a plateau phase followed by a decreased fluorescence signal, probably due to the consumption of furin and photobleaching of the fluorophore Edans, respectively. To investigate whether a higher furin concentration provides more-efficient cleavage, all peptides were also incubated with 20 nM furin. The incubation with the enhanced furin concentration resulted in an increased conversion of the peptides. As a result of the lower cleavage rate of P8-L and P8-S, these peptides still displayed significantly lower RFU values than P8-P and P8-T (Fig. 3c).

The ability to mediate cell-to-cell fusion does not correlate with the efficiency of virus-induced fusion between viral and cellular membranes. To investigate the F-mediated fusion between viral and cellular membranes, viral pseudotypes bearing the MuV F and HN glycoproteins were generated and the transduction of Vero76 cells was analyzed. The total yield of Vesicular stomatitis virus (VSV) pseudotype particles (VSVpp) harboring viral glycoproteins of Urabe AM9 was very low; therefore, Urabe AM9 pseudotypes were concentrated by centrifugation before they were subjected to Western blotting and transduction studies.

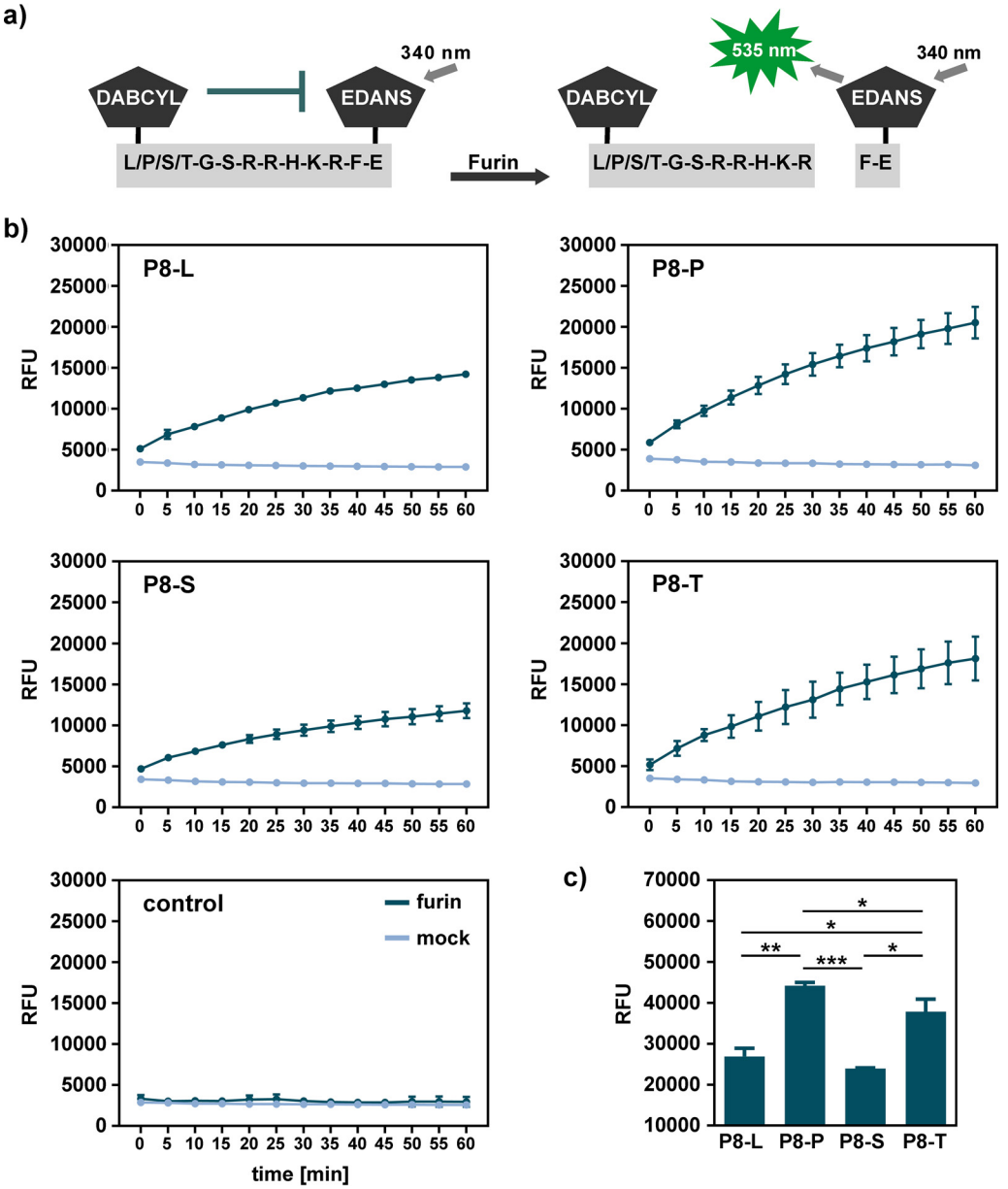

FIG 3 Efficiency of proteolytic cleavage by furin. (a) Schematic illustration of FRET peptides before and after proteolysis by furin. (b) FRET peptides were incubated without (mock) or with 10 nM furin. Assay buffer harboring no peptide was used as a control. Proteolytic cleavage was quantified by measuring the fluorescence signal using an excitation wavelength of 340 nm and an emission wavelength of 535 nm and is given as relative fluorescence units (RFU). The graphs show means and SDs from three independent trials. (c) FRET peptides were incubated with 20 nM furin, and the cleavage efficiency was determined by measuring the fluorescence signal using an excitation wavelength of 340 nm and an emission wavelength of 535 nm. The graph shows means and SDs from three independent experiments. Statistical significance was tested by paired, two-tailed Student's *t* test with 95% confidence intervals. *, $P \leq 0.05$; **, $P \leq 0.01$; ***, $P \leq 0.005$.

The incorporation of MuV F into VSVpp was analyzed by Western blotting to ensure that similar amounts of surface-expressed MuV F P8-L, -P, -S, and -T were incorporated into the pseudoviral particles. For each strain, the quantity of VSVpp shown by the detection of VSV N and the amount of incorporated F proteins were similar regardless of the amino acid residue present at P8, as indicated by the comparable intensities of protein bands (Fig. 4a). No differences were obtained regarding the cleavability when comparing the four variants for each strain. For all strains, F was mainly detected as the cleaved F_1 subunit at a molecular weight of approximately 55 to 50 kDa. The molecular weight of 88-1961 F was slightly higher than those of ZK-BN and Urabe AM9 F, probably

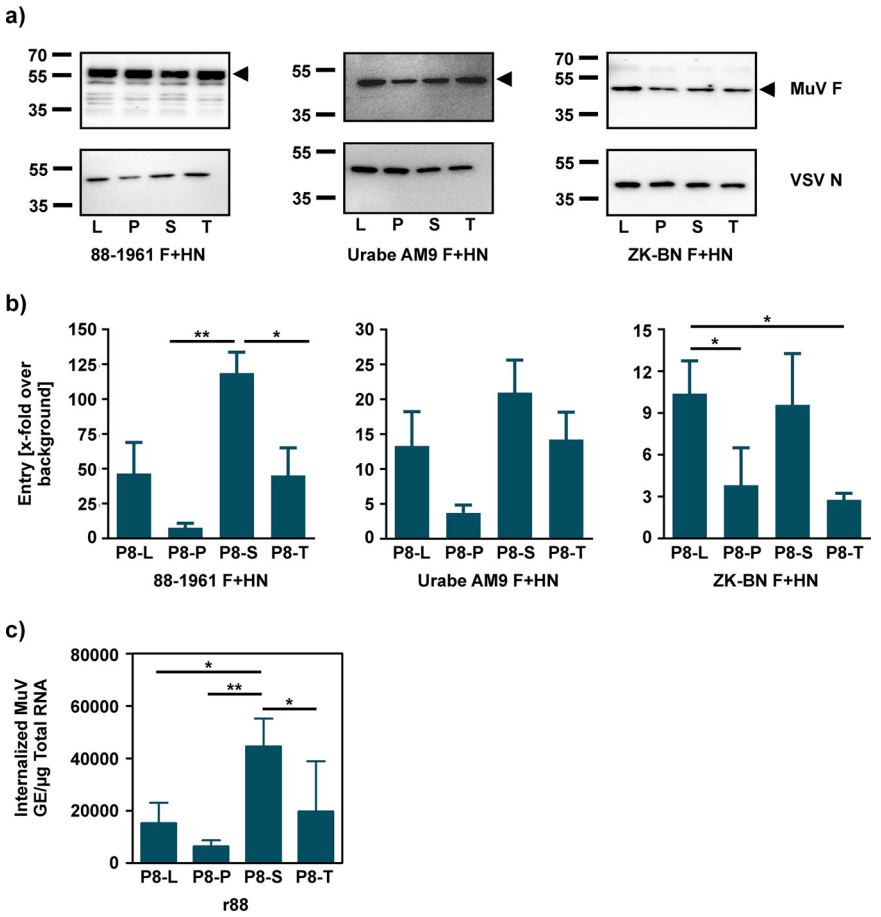

FIG 4 MuV F-mediated entry. (a) Lysates of purified VSV pseudotypes harboring MuV F and HN glycoproteins were subjected to SDS-PAGE and Western blotting under reducing conditions. F proteins were detected by incubation with antibodies directed against the cytoplasmic tail of MuV F; VSV-N served as a loading control. Arrow heads indicate F_1. Molecular mass (kDa) is indicated on the left. Exposure times: 88-1961 MuV F, 20 s; 88-1961 VSV-N, 2 s; Urabe AM9 MuV F, 5 s; Urabe AM9 VSV N, 1 s; ZK-BN MuV F, 90 s; ZK-BN VSV N, 3 s. (b) Vero76 cells were inoculated with VSV pseudotypes harboring no viral glycoprotein (pCG1) or MuV HN and F variants as indicated. At 16 h postinoculation, F- and HN-driven entry was quantified by measuring the luciferase activity in cell lysates and is given as x-fold transduction over background. The graphs show means and SDs from four independent experiments. Statistical significance was tested by paired, two-tailed Student's *t* test with 95% confidence intervals. *, $P \leq 0.05$; **, $P \leq 0.01$. (c) Internalization of r88. Cells were inoculated with r88 P8-L/P/S/T at an MOI of 0.5. Viral internalization was quantified by qRT-PCR and is given as MuV GE/μg total RNA. The graph shows means and SDs from four independent experiments. Statistical significance was tested by paired, two-tailed Student's *t* test with 95% confidence intervals. *, $P \leq 0.05$; **, $P \leq 0.01$.

due to differences in the glycosylation status. For the F proteins of the 88-1961 strain, multiple protein bands with a molecular weight ranging from approximately 50 to 30 kDa were additionally detected and might represent either premature products of F or protein fragments that occurred due to the sample preparation. The F/HN-driven entry of VSVpp varied depending on P8 and was contrariwise to the results obtained for the cell-to-cell fusion. For all strains, weak transduction levels were obtained for F P8-P, although this variant is highly efficient in inducing cell-to-cell fusion and exhibits the fastest proteolytic conversion rate for furin (Fig. 4b). In contrast, more-efficient entry of VSVpp was mediated by F P8-S—a protein that is cleaved much more slowly than F P8-P and induces less syncytium formation following overexpression. For VSVpp harboring glycoproteins of 88-1961 or Urabe AM9, P8-L and P8-T displayed similar intermediate values. In the case of ZK-BN, P8-T showed low transduction levels, whereas the highest transduction level was obtained for P8-L.

To investigate the effect of P8 in the context of MuV virions, internalization assays were performed using a recombinant variant of the 88-1961 MuV strain harboring

the respective amino acid residues at P8 (r88 P8-L, -P, -S, and -T), and viral entry was quantified by measuring the number of genome equivalents (GE) via reverse transcription-quantitative PCR (qRT-PCR). Consistent with the results obtained by the transduction experiments, the highest number of internalized MuV particles was observed for r88 P8-S (44,593.2 GE/μg total RNA), whereas r88 P8-P displayed the lowest (6,338.7 GE/μg total RNA) (Fig. 4c).

P8-L and P8-S reduce virus-induced cytopathic effects. To investigate the impact of the amino acid residue at P8 on viral replication, the release and spread of wild-type (wt; r88 P8-P) and modified versions of r88 in which the amino acid residue at P8 has been altered to L, S, or T were analyzed. For all recombinant MuVs, the expression levels of the respective F proteins were comparable. In line with the results observed for MuV F incorporation into VSVpp, all r88 F proteins were detected as their cleaved F_1 subunit at a molecular weight of approximately 60 kDa regardless of the amino acid residue at P8 (Fig. 5a). For all viruses, only single infected cells were detected at 1 day postinfection (dpi) (Fig. 5b). At 2 dpi, infection by r88 P8-P, P8-S, and P8-T was widespread, whereas r88 P8-L showed restricted spread in small foci. Syncytia were detected for all four viruses but were less prominent for r88 P8-L. The infection with r88 P8-T resulted in the detachment of infected cells and vacuolization of virus-induced syncytia at 2 dpi. In accordance with the data obtained for the coexpression of 88-1961 F and HN, r88 P8-P and r88 P8-T exhibited increased fusogenicity compared to that of r88 P8-L and r88 P8-S, as indicated by the higher number and size of syncytia (Fig. 5c; Table 2). Consistent with the results obtained by the microscopic evaluation of virus-induced cytopathic effects (CPEs), the viability of cells infected with r88 P8-P or r88 P8-T decreased significantly at 2 dpi, whereas no or only a minor negative effect on cell viability was observed for r88 P8-L and r88 P8-S, respectively (Fig. 5d).

When focusing on the release of viral particles from infected cells, r88 P8-P and P8-L showed similar growth kinetics, although the number of infected cells was lower for r88 P8-L. Peak titers of 4.4×10^6 PFU/ml (r88 P8-P) and 4.7×10^6 PFU/ml (r88 P8-L) were reached at 3 dpi (Fig. 6a). r88 P8-S displayed similar titers at 1 and 2 dpi, followed by approximately 10-fold lower titers during the remaining days. Viral titers of r88 P8-T were constantly lower than r88 P8-P and r88 P8-L, probably as a consequence of the severe virus-induced CPEs and the resulting apoptosis and detachment of cells. In addition to determining the titers of released viral particles, the intracellular viral titers of infected cells were investigated. At 1 dpi, intracellular titers of r88 P8-P and r88 P8-T were comparable to the released viral titers obtained for the same viruses, whereas the intracellular titers of r88 P8-L and r88 P8-S were slightly lower than the titers of released viral particles (Fig. 6b). This effect was even more prominent at 2 dpi: the titers for cell-free viruses were approximately 23-fold higher than the intracellular titers for r88 P8-L and r88 P8-S. In comparison, intracellular titers for r88 P8-P and r88 P8-T were only 5.4- and 3.1-fold lower than the titers for cell-free viruses.

Proteolytic activation of MuV F depends on processing by the cellular protease furin. It was previously shown that the inhibition of the host cell protease furin leads to decreased MuV titers (28). To analyze whether the amino acid residue at P8 affects the dependence of MuV F proteolysis on the cellular protease furin in a viral context, viral release of r88 P8-L/P/S/T was compared in the presence and absence of the furin inhibitor MI-1148. Regardless of the amino acid residue present at P8, the inhibition of furin reduced the viral titers to 4×10^1 to 2.5×10^2 PFU/ml (Fig. 6c), indicating that the proteolytic processing of MuV F critically depends on cleavage by furin irrespective of the amino acid residue at P8.

DISCUSSION

MuV infections lead to the highly infectious disease mumps that is characterized by the typical parotitis and mild flu-like symptoms (1). In some cases, severe complications, including pancreatitis, orchitis, or myocarditis, may occur (1, 29, 30). Clinical MuV isolates have a differently pronounced neurovirulent potential, and the central nervous

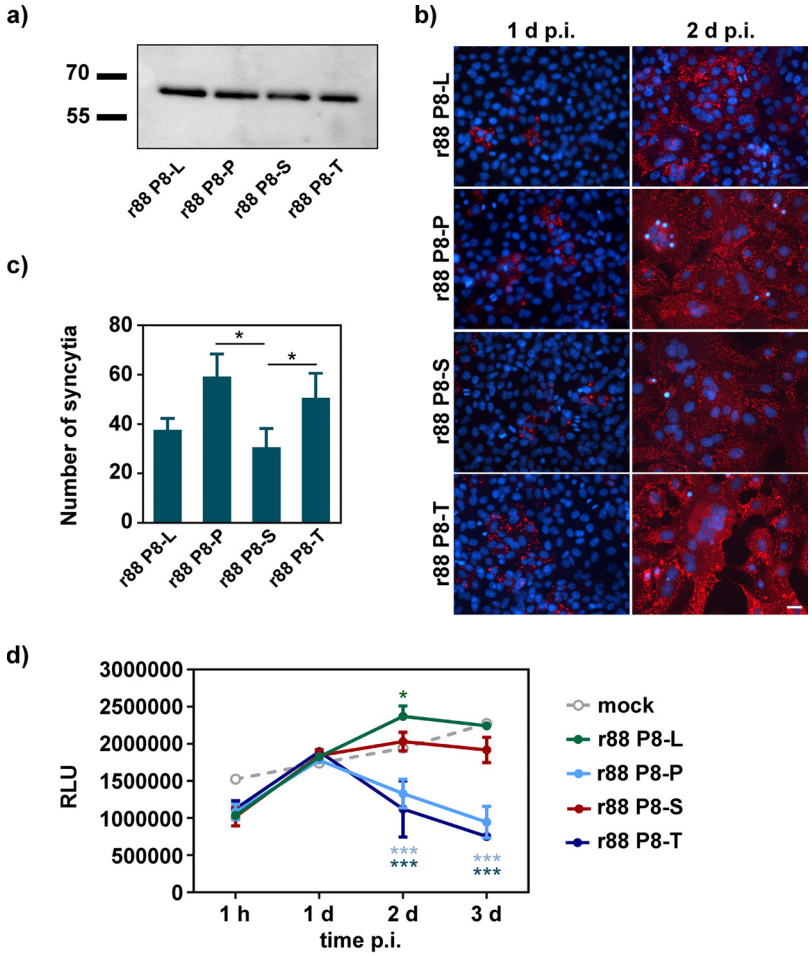

FIG 5 Virus-induced cytopathic effects. (a) Expression and cleavage of r88 F. Lysates of purified r88 were separated by SDS-PAGE under reducing conditions. F proteins were detected by incubation with antibodies directed against the cytoplasmic tail of MuV F and HRP-conjugated anti-rabbit antibodies. Exposure time: 50 s. Molecular mass (kDa) is indicated on the left. (b) Spread of infection in Vero76 cells. Cells were fixed at 1 and 2 dpi. MuV-infected cells were detected by incubation with an antiserum directed against MuV Kilham strain and Alexa Fluor 594-conjugated secondary antibodies. Nuclei were stained with DAPI. Scale bar, 25 μm. (c) Virus-induced syncytium formation at 1 dpi. The total numbers of syncytia per coverslip were counted. Syncytia were defined as multinucleated cells that harbored at least three nuclei and showed a positive fluorescence signal for viral proteins of r88. The graph shows means and SDs from three independent experiments. Statistical significance was tested by paired, two-tailed Student's *t* test with 95% confidence intervals. *, $P \leq 0.05$. (d) Virus-induced cytopathic effect. Cells were infected with r88 P8-L/P/S/T, and cellular ATP was measured at 1 hpi and 1, 2, and 3 dpi. Uninfected cells served as a control. The graph shows means and SD of three independent experiments. Statistical significance compared to mock-infected control was tested by two-way analysis of variance (ANOVA) and Bonferroni posttests. *, $P \leq 0.05$; ***, $P \leq 0.005$.

system (CNS) is involved in half of all cases (30–32). In rare cases, the CNS involvement can even result in lethal meningitis, encephalitis, or hydrocephalus formation (2, 3). MuV strains and isolates differ in their ability to mediate cell-to-cell fusion, and a correlation between virulence and fusogenicity has been suggested (9, 20, 21, 33–35).

TABLE 2 Syncytium formation in Vero76 cells following infection with r88 at 1 dpi[a]

Virus	No. of syncytia	No. of nuclei per syncytium	Total no. of nuclei in fusion
r88 P8-L	37.7	9.9	370
r88 P8-P	59.3	13.6	721.3
r88 P8-S	30.6	12.1	420.3
r88 P8-T	50.7	16.2	818.7

[a]The values are means from three independent experiments.

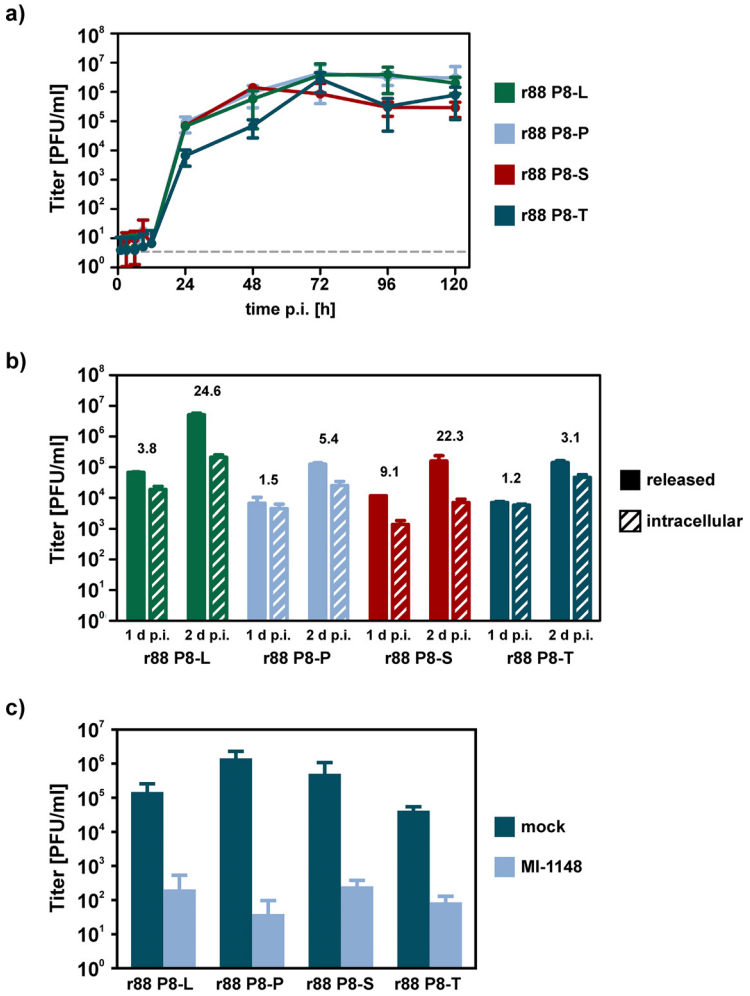

FIG 6 Replication of MuV 88-1961 harboring L, P, S, or T at P8. (a) Multistep viral growth kinetics in Vero76 cells. Cells were infected at an MOI of 0.01, and supernatants were collected at the indicated time points. Viral titers were determined by titration on Vero76 cells and are given as PFU per milliliter. The graph shows means and SDs from three independent experiments. The dashed line indicates the limit of detection. (b) Intracellular viral titers of infected Vero76 cells. Cells were infected at an MOI of 0.01. Intracellular viruses were released by freeze-thaw treatment at 1 and 2 dpi. Intracellular titers and titers of released viral particles were determined by titration on Vero76 cells and are given as PFU per milliliter. The graph shows means and SDs from three independent experiments. Numbers indicate the multiplicity of released viral titers compared to intracellular titers. (c) Vero76 cells were infected with r88 P8-L/P/S/T at an MOI of 0.01 in the absence (mock) or presence of 10 μM furin inhibitor MI-1148. Viral titers were determined at 2 dpi by titration on Vero76 cells. The graph shows means and SDs from three independent experiments.

So far, the reasons for the differential fusogenicity and the importance for MuV pathogenesis are unclear.

The proteolytic activation of MuV F by the subtilisin-like proprotein convertase furin is essential for the priming of the fusion-inactive F_0 precursor protein and occurs at a multibasic cleavage motif (R-R-H-K-R) (12). Recently, it was suggested that not only the narrow cleavage motif but a total of 20 aa residues may play an important role for the accessibility of the proteolytic cleavage motif by furin (36).

Here, we focused on the amino acid residue present at P8 of the cleavage motif of MuV F proteins, given that a total of four different residues (L, P, S, and T) can be found at this position depending on the MuV genotype. We demonstrate that the amino acid residue at P8 affects the kinetics of MuV F proteolysis by furin and modulates the extent of F-induced cell-to-cell fusion and virus-induced CPE development. The cleavage rate as well as the ability to mediate cell-to-cell fusion decreases when L or S is present at

P8, suggesting that the impaired fusogenicity is a result of the delayed F activation. Previous studies strengthen our observation that the extent of F-induced cell-to-cell fusion is affected by the amino acid residue at P8. The Jeryl Lynn vaccine strain (genotype A, P8-L) exhibits only weak fusogenic properties and is not associated with neurological disease; similarly, the avirulent RW strain (genotype D, P8-L) does not cause obvious cytopathic effects, and the Enders and SBL strains (both genotype A, P8-L) have no neurovirulence potential (20, 37). The vaccine strains Leningrad-3 and Leningrad-Zagreb (genotype N, P8-P) that have led to neurological complications in the past as well as most of the currently circulating MuV strains, including the highly neurovirulent strain 88-1961, harbor a P at P8 (38–40).

The longest substrate analogue inhibitor used for crystallization and structure determination in complex with furin comprises only the P6 to P1 segment (41). So far, no information regarding the exact position of the P8 residue in furin substrates is available. Although the P8 residue should be located outside the active site, it might have an influence on the efficiency of proteolytic cleavage by furin (36). However, crystal structures of uncleaved F_0 proteins are needed to reveal the influence of P8 modifications on the binding of MuV F to furin. The generation of MuV F crystals in complex with furin is challenging, and so far, there is only information about the crystal structure of the MuV F core region (heptad-repeat regions HRA and HRB) available (42, 43). Nevertheless, it has been reported that the amino acid residue present at P12 affects viral fusogenicity and neurovirulence, emphasizing the importance of the cleavage motif for MuV infectivity and virulence (24).

Furin undergoes cellular trafficking and is transported from the *trans*-Golgi network (TGN) to the cell surface and back to the TGN via the endosomal pathway (44, 45). It is known that cell surface furin activates various bacterial and viral pathogens, including *Bacillus anthracis* toxin, *Clostridium septicum* toxin, certain hemagglutinins of highly pathogenic avian influenza viruses, Dengue virus prM, and human papillomavirus minor capsid protein L2 (15, 46–51). The cleavage of MuV F by furin mainly occurs during its maturation in the TGN within the infected cell (12–15). For MuV F P8-P and P8-T, fast proteolytic cleavage might result in the expression of cleaved F proteins on the surface of transfected or infected cells, thus enabling a direct fusion with neighboring cells. Vice versa, the slower and therefore less efficient intracellular cleavage of MuV F P8-L and P8-S leads to a larger proportion of uncleaved F proteins on the cell surface, prohibiting the subsequent cell-to-cell fusion. Given that these viruses are still able to mediate fusion with the plasma membrane, it is very likely that uncleaved MuV F P8-L and P8-S proteins are proteolytically activated by cell surface furin during the entry process into new target cells. Consequently, the proteolytic activation on the cell surface allows F-mediated fusion between viral and cellular membranes and spread of infection without inducing severe cytopathic effects such as the formation of syncytia. However, the cleavage of MuV F P8-L and P8-S on the surface of transfected cells does not allow the induction of F-mediated cell-to-cell fusion comparable to that of MuV F P8-P and P8-T. Further, viral entry—specifically, the fusion between viral and host cell membranes—is more efficient for F P8-L or P8-S, suggesting that cell-to-cell and virus-cell fusion might require different conditions. The presence of L or S at P8 might provide conditions that are beneficial for virus-cell fusion, whereas for P or T, cell-to-cell fusion is more efficient. This assumption is encouraged by the observation that MuVs harboring P8-L or P8-S yield higher titers of cell-free virus than intracellular virus. It was previously shown for several viruses, including mouse hepatitis coronavirus, Sendai virus, herpesviruses, and human immunodeficiency virus type 1, that virus-induced fusion between neighboring cells or between viruses and cells seems to represent two unequal processes with different requirements, although the underlaying mechanisms are not fully understood (52–57).

In sum, our findings demonstrate that one single amino acid residue close to the cleavage motif of MuV F affects the proteolytic processing as well as the extent and type of F-induced fusion (cell-to-cell versus virus-cell). The way of spread plays an important role for virulence. Although cell-free spread enables a rapid distribution

through body fluids within the infected organism, free viral particles are exposed to various barriers of infection such as components of the hosts' innate immune defense, macrophages, or physical barriers, e.g., the blood-brain barrier. In contrast to this, cell-to-cell spread allows direct infection of neighboring cells and bypassing of the barriers mentioned before (58–62). Also, it has been assumed that the ability of MuV to mediate cell-to-cell fusion correlates with virulence, and the majority of highly virulent field isolates are highly fusogenic *in vitro* (9, 20, 21, 33–35). As P8 plays an important role for virus-induced fusogenicity and spread of infection, the amino acid residue at this particular position might be used as a virulence marker to predict the virulence of newly arising strains.

MATERIALS AND METHODS

Sequence homology analysis. A total of 201 full-length MuV genomes were used for sequence analysis. The amino acid sequences of the F proteins were aligned, and consensus sequences for each genotype as classified by the nucleotide sequence of the SH proteins were generated using the BioEdit sequence alignment editor. Information on the MuV strains used for sequence analysis and an overview of the proteolytic cleavage motif of each strain are given in Data Set S1 in the supplemental material.

Cell lines. Vero76 (African green monkey, kidney) and HEK-293T (human, kidney, ATCC: CRL-3216) cells were maintained in Dulbecco's minimum essential medium (DMEM; GIBCO) supplemented with 5% fetal calf serum (FCS; Sigma-Aldrich). BSR-T7/5 cells (BHK-21 cell clone constitutively expressing T7 RNA polymerase) (63) were maintained in DMEM supplemented with 10% FCS, 2% nonessential amino acids (Thermo Fisher Scientific), and 1 mg/ml Geneticin (Thermo Fisher Scientific). All cells were cultivated in 75-cm² tissue culture flasks (Greiner Bio-One) at 37°C and 5% CO_2.

Expression plasmids. Expression plasmids coding for the wild-type (wt) F and HN proteins of the human MuV strains MuVi/1961.USA/0.88[H] (88-1961; GenBank accession number AF467767.2) (40), Urabe AM9 (GenBank accession number FJ3757185.1) (64), and ZK-BN/H-0001 (ZK-BN; GenBank accession numbers KM519599 [F] and KM519600 [HN]) (27) were generated by cloning the respective open reading frame (ORF) into the expression vector pCG1 (65) using BamHI and SalI restriction sites. For detection by immunostaining, all F proteins were fused to a C-terminal hemagglutinin (HA) epitope (YPYDVPDYA), whereas the HN proteins were fused to a FLAG epitope (DYKDDDDK) at the C-terminal end. In addition, plasmids coding for F proteins in which the amino acid residue at position 95 was modified by site-directed mutagenesis were generated: 88-1968 F P8-L/S/T, Urabe AM9 F P8-L/P/T, and ZK-BN F P8-L/S/T.

In addition, cDNA plasmids harboring the full-length cDNA of human MuV 88-1961 in which the nucleotides coding for the amino acid residue at position 95 of the F protein were altered by site-directed mutagenesis were generated and cloned into the expression vector pBlueScript II SK(+). The following nucleotides were exchanged: C4829 to T (r88 P8-L), C4828 to T (r88 P8-S), and C4828 to A (r88 P8-T). Plasmids expressing the 88-1961 N, P, and L gene products had already been generated and were described in previous studies (23, 66). All plasmids were verified by automated sequencing (Eurofins Genomics GmbH).

Rescue of recombinant viruses. The rescue of recombinant MuVs was performed as described recently (28, 66). Briefly, BSR-T7/5 cells (63) were transfected with full-length MuV 88-1961 cDNA plasmids and the corresponding helper plasmids N, P, and L. Virus-containing BSR-T7/5 supernatants were collected as a widespread cytopathic effect (CPE) occurred and subsequently loaded onto Vero76 cells for further propagation. Depending on the occurrence of syncytia and/or a widespread CPE, supernatants were collected, centrifuged at 2,100 rpm and 4°C for 10 min, and stored at −80°C. Viral RNA was extracted from Vero76 cell culture supernatants using the QiAMP MinElute Virus Spin kit (Qiagen), followed by reverse transcriptase PCR using random primers and SuperScript II reverse transcriptase (Life Technologies). cDNA fragments were amplified and verified by automated sequencing (Eurofins Genomics GmbH) to exclude any spontaneous mutations during the rescue process.

Fusion assay and immunofluorescence microscopy. Cells were seeded on coverslips and transfected with 1 μg of expression plasmids coding for wild-type MuV F (88-1961 F P8-P, Urabe AM9 P8-S, and ZK-BN P8-P) or MuV F in which the amino acid residue at P8 had been altered (88-1961 F P8-L/S/T, Urabe AM9 F P8-L/P/T, and ZK-BN F P8-L/S/T) and 1 μg of expression plasmids coding for the corresponding MuV HN using the ICAFectin 441 transfection reagent (In-Cell-Art) according to the manufacturer's protocol. At 1 day posttransfection (dpt), cells were fixed with 4% paraformaldehyde (PFA) and permeabilized with 0.2% Triton X-100 (Sigma-Aldrich). Epitope-labeled F and HN proteins were detected by incubation with antibodies directed against the HA (dilution, 1:500; mouse [Sigma-Aldrich]) or FLAG (dilution, 1:500; rabbit [Sigma-Aldrich]) epitope in a humidity chamber for 1 h. For visualization, incubation with Alexa Fluor 594-/488-conjugated secondary antibodies (dilution, 1:1,000; Life Technologies) directed against mouse or rabbit primary antibodies was performed in a humidity chamber for 30 min. Finally, nuclei were visualized by incubation with 4′,6-diamidino-2-phenylindole (DAPI; Carl Roth GmbH + Co. KG), and coverslips were mounted in ProLong Gold antifade mountant (Thermo Fisher Scientific). Cells were analyzed for the presence of syncytia using a Nikon Eclipse Ti microscope and the NIS Elements AR imaging software (Nikon Instruments). Syncytia were defined as multinucleated cells that harbored at least three nuclei and were positive for the expression of both MuV glycoproteins. The total number of syncytia per coverslip and the number of nuclei in each syncytium were counted to calculate the cumulative number of nuclei in syncytia per coverslip.

VSV pseudotypes. A replication-deficient Vesicular stomatitis virus (VSV) vector that codes for an enhanced green fluorescent protein (eGFP) and a firefly luciferase instead of the VSV glycoprotein G (VSV*ΔG-fLuc) was employed for the generation of rhabdoviral pseudotypes as previously described (67–69). Briefly, HEK-293T cells were grown in 6-well plates and transfected with expression plasmids encoding no viral glycoprotein (pCG1, negative control), VSV G (positive control), or MuV F+HN by calcium-phosphate precipitation. At 16 h posttransfection (hpt), cells were inoculated with VSV*ΔG-fLuc for 1 h at 37°C, washed with phosphate-buffered saline (PBS) three times, and incubated with anti-VSV antibody containing cell culture supernatants of I1 hybridoma cells (ATCC CRL-2700) (70). At 1 day postinoculation, supernatants were collected, centrifuged to remove cell debris, and further used for SDS-PAGE and Western blotting or the transduction of Vero76 cells. For transduction, Vero76 cells were seeded in clear 96-well plates. After reaching confluence, cells were inoculated with VSV pseudotypes (VSVpp) for 16 h at 37°C. VSVpp harboring Urabe AM9 F and HN glycoproteins were generated in 75-cm^2 cell culture flasks and 10-fold concentrated by centrifugation through Vivaspin centrifugation filters with a cutoff of 35 kDa (Sartorius). To quantify the transduction efficiency of VSVpp harboring MuV glycoproteins, cells were lysed by incubation with cell culture lysis reagent (Promega) for 30 min at room temperature and transferred into white 96-well plates. Luciferase activity was measured using the Beetle-Juice kit (PJK GmbH) and a GENios pro chemiluminometer (Tecan) according to the manufacturer's protocols.

Viral growth kinetics and titration. Vero76 cells were grown in 24-well plates until reaching confluence and infected with recombinant human MuV strain 88-1961 (r88) as well as modified viral clones in which the amino acid residue at position 95 within the F protein has been modified (r88 P8-L/S/T) at a multiplicity of infection (MOI) of 0.01 for 1 h at 37°C. The inoculum was removed, and cells were washed with PBS three times before 1.25 ml of cell culture medium was added to the cells. One hundred twenty-five microliters of the supernatants were collected at 1, 3, 6, 9, and 12 h postinfection (hpi) as well as 1 to 5 dpi and immediately stored at −80°C until further usage. The removed supernatants were replaced by the same volumes of fresh cell culture medium. To determine viral titers, Vero76 cells were grown in 12-well plates until reaching confluence. Cells were infected with 10-fold serial dilutions of virus-containing supernatants for 1 h at 37°C. The inoculum was removed, and cells were washed with PBS and finally overlaid with 1% plaque agarose (Biozym Scientific GmbH) solved in Eagle's minimal essential medium without phenol red (Lonza) supplemented with 5% FCS. Cells were fixed with 4% PFA overnight after virus-induced plaques occurred. The agarose was removed, and cells were incubated with 0.1% crystal violet (Merck KGaA) diluted in Aqua Bidest at room temperature for 10 min. Cells were washed, and viral titers were determined by counting the number of virus-induced plaques in each well and multiplying it with the reciprocal of the dilution factor and the volume used for infection. Viral titers are given in PFU per milliliter.

To determine intracellular viral titers, infected cells were stored on ice and washed three times with ice-cold PBS. Next, cells were removed from the well plates by using a cell scraper and transferred into reaction tubes. Cells were washed by centrifugation at 2,400 rpm and 4°C for 10 min, the supernatants were removed, and the cell pellets were resuspended in ice-cold PBS. After three washing steps, cells were resuspended in 100 μl PBS and frozen at −80°C overnight. The next day, cells were thawed and centrifuged at 2,400 rpm and 4°C for 10 min. The supernatants were collected, filtrated (pore size, 0.2 μm), and used for plaque assay as described above to determine the intracellular viral titer.

In addition, cells were grown on coverslips and infected as described above. At 1 and 2 dpi, cells were fixed and permeabilized, and viral proteins were detected by incubation with neutralizing antibodies directed against MuV Kilham strain (dilution, 1:500; rabbit) (71), followed by incubation with Alexa Fluor 594-conjugated secondary antibodies directed against rabbit IgG (dilution, 1:1,000; Life Technologies). Cells were analyzed for the presence of syncytia by using a Nikon Eclipse Ti microscope and the NIS Elements AR imaging software (Nikon Instruments). Syncytia were defined as multinucleated cells that harbored at least three nuclei and were positive for the presence of viral proteins of r88. The total number of syncytia per coverslip and the number of nuclei in each syncytium were counted to calculate the cumulative number of nuclei in syncytia per coverslip.

Viral toxicity assay. Virus-induced cell damage was determined by measuring cellular ATP of infected cells using the Viral ToxGlo kit (Promega). Cells were seeded in white 96-well plates until reaching confluence. Next, cells were infected with r88 P8-L/P/S/T at an MOI of 0.1 for 1 h at 37°C. Uninfected cells served as a control for maximal vitality. At 1 hpi and 1 to 3 dpi, 100 μl of the ATP detection reagent was added. Next, the plate was shaken for 2 min and further incubated for 10 min at room temperature followed by measuring the luminescent signal using a GENios pro chemiluminometer (Tecan).

Internalization assay and qPCR. Vero76 cells were inoculated with r88 P8-L/P/S/T at an MOI of 0.5 and incubated for 1 h at 4°C. The inoculum was removed, and cells were washed three times with PBS. Cells were further incubated in DMEM for 90 min at 37°C. DMEM was removed, and cells were washed three times with PBS, followed by an incubation with trypsin until cells detached. Trypsinization was stopped by adding FCS. Next, cells were transferred into reaction tubes and collected by centrifugation at 600 × *g* for 10 min at room temperature. Supernatants were removed, and the cell pellets were resuspended in PBS, followed by an additional centrifugation step. Cell pellets were further used for RNA extraction using TRIzol reagent (Thermo Fisher Scientific). Reverse transcriptase PCR was performed using random primers and SuperScript III reverse transcriptase (Thermo Fisher Scientific). cDNA was subjected to qPCR using SYBR green master mix (Thermo Fisher Scientific) and primers targeting r88 L (forward, TGCTTCCTAACAACCGACCT; reverse, GAGGGTTGAAGGGATCACCA). Cycle threshold (C_T) values of r88 were normalized to total RNA. Dilution series of the expression plasmid pBlueScript II SK(+) containing

the full-length cDNA of r88 were used as standards to calculate the amount of genomic equivalents (GE) based on the C_T values.

Inhibition of cellular furin. Cells were incubated with 10 μM furin inhibitor MI-1148 (4-guanidinomethyl-phenylacetyl-Arg-tert.Leu-Arg-4-amidinobenzylamide) (72) for 3 h prior transfection or infection. Next, transfection or infection was performed as described before. Cells were washed and further incubated with cell culture medium containing 10 μM MI-1148 for 1 (transfection) or 2 (infection) days. Cells were further subjected to immunofluorescence analysis, and viral titers were determined by titration on Vero76 cells.

SDS-PAGE and Western blotting. Cell culture supernatants containing VSVpp or r88 were loaded onto a 20% sucrose cushion in PBS and centrifuged at 17,000 $\times$ *g* for 2 h at 4°C. The pellets were resuspended in 2$\times$ SDS-containing lysis buffer supplemented with β-mercaptoethanol. Samples were heated for 10 min at 96°C before the lysates were loaded onto SDS gels (10% SDS) for SDS-PAGE and Western blotting.

Transfected cells were washed with ice-cold PBS and incubated with 0.5 mg/ml LC biotin (Thermo Fisher Scientific) for 15 min at 4°C. Next, cells were washed with PBS-0.1 M glycine and further incubated for 15 min at 4°C. Cells were rinsed from the bottom of the plates, transferred into reaction tubes, and centrifuged. The cell pellet was resuspended in PBS, and cells were homogenized by centrifugation through a QIAshredder column (Qiagen) for 1 min at 13,000 rpm two times. Samples were either mixed with 2$\times$ SDS buffer supplemented with β-mercaptoethanol to detect total amounts of MuV F or loaded onto streptavidin-agarose (Pierce) and incubated overnight on an overhead shaker. Agarose-bound samples were centrifuged for 5 min at 13,000 rpm at 4°C, the supernatants were removed, and the proteins were washed with PBS. This washing step was repeated three times before the samples were mix with 2$\times$ SDS buffer supplemented with β-mercaptoethanol. Samples derived from transfected cells were incubated at 56°C for 5 min before they were loaded onto SDS gels.

MuV F proteins incorporated into VSVpp or r88 were detected by incubation with antibodies directed against the cytoplasmic tail of MuV F (dilution, 1:500; rabbit) (27) followed by incubation with horseradish peroxidase (HRP)-conjugated secondary antibodies (dilution, 1,1000; Dako GmbH). VSV nucleoprotein (N) was detected by anti-VSV N antibodies (dilution, 1:250; rabbit) and HRP-conjugated secondary antibodies (dilution, 1:1,000; Dako GmbH). To detect F proteins expressed in transfected cells, membranes were incubated with antibodies directed against the HA epitope (dilution, 1:1,000; rabbit [Sigma-Aldrich]) followed by incubation with anti-rabbit HRP-conjugated secondary antibodies. β-Catenin was detected by anti-β-catenin antibodies (dilution, 1:1,000; mouse [Abcam]) and HRP-conjugated secondary antibodies (dilution, 1:1,000; Dako). For the visualization of protein bands, membranes containing the immobilized proteins were incubated with SuperSignal West Dura extended duration substrate (Thermo Fisher Scientific), placed in a ChemiDoc imager, and analyzed with the Image Lab software (Bio-Rad).

Fluorescence resonance energy transfer assay. To determine whether the amino acid residue at P8 has an influence on the proteolytic cleavage by the host cell protease furin, peptides corresponding to the amino acid residues P8 to P1′ were flanked by the donor-quencher pair Edans-Dabcyl (Peptides & Elephants GmbH) and subjected to a fluorescence resonance energy transfer (FRET) assay (Fig. 3a). Proteolytic cleavage of peptides was measured in black 96-well plates at room temperature by a GENios pro chemiluminometer (Tecan). Each well contained 190 μl of assay buffer (50 nM HEPES, 154 nM NaCl, 2 mM $CaCl_2$, 2% ethanol, pH 7.4), 20 μM substrate, and 10 or 20 nM recombinant human furin (R&D Systems). Proteolytic cleavage was quantified by measuring the fluorescence signal of the donor-quencher pair every 5 min for a total timespan of 1 h using an excitation wavelength of 340 nm and an emission wavelength of 535 nm. Wells containing only buffer or buffer with substrate/enzyme alone served as controls to define the background signal.

Statistical analysis. To determine statistical significance, paired, two-tailed Student's *t* tests were used for combined data from multiple experiments. Statistical analysis was performed using GraphPad Prism 5.03 software. Statistical details of each experiment can be found in the corresponding figure legend.

SUPPLEMENTAL MATERIAL

Supplemental material is available online only.

SUPPLEMENTAL FILE 1, XLSX file, 0.1 MB.

ACKNOWLEDGMENTS

We thank Karl-Klaus Conzelmann (LMU Munich) for providing BSR-T7/5 cells.

This research was funded by the German Research Foundation (DFG), grant number KR-4762/2-1. The funders had no role in the design of the study, in the collection, analyses, or interpretation of data, in the writing of the manuscript, or in the decision to publish the results.

We declare no conflict of interest.

Conceptualization, N.K.; investigation, S.H., M.H., and N.K.; formal analysis, S.H., M.H., and N.K.; resources, T.S. and C.S.; writing – original draft preparation, S.H. and N.K.; writing – review and editing, all authors; funding acquisition, N.K. All authors have read and agreed to the published version of the manuscript.

REFERENCES

1. Beard CM, Benson RC, Jr, Kelalis PP, Elveback LR, Kurland LT. 1977. The incidence and outcome of mumps orchitis in Rochester, Minnesota, 1935 to 1974. Mayo Clin Proc 52:3–7.
2. Russell RR, Donald JC. 1958. The neurological complications of mumps. Br Med J 2:27–30. https://doi.org/10.1136/bmj.2.5087.27.
3. Rubin S, Eckhaus M, Rennick LJ, Bamford CG, Duprex WP. 2015. Molecular biology, pathogenesis and pathology of mumps virus. J Pathol 235:242–252. https://doi.org/10.1002/path.4445.
4. Elango N, Varsanyi TM, Kovamees J, Norrby E. 1988. Molecular cloning and characterization of six genes, determination of gene order and intergenic sequences and leader sequence of mumps virus. J Gen Virol 69:2893–2900. https://doi.org/10.1099/0022-1317-69-11-2893.
5. Paterson RG, Lamb RA. 1990. RNA editing by G-nucleotide insertion in mumps virus P-gene mRNA transcripts. J Virol 64:4137–4145. https://doi.org/10.1128/JVI.64.9.4137-4145.1990.
6. Kubota M, Takeuchi K, Watanabe S, Ohno S, Matsuoka R, Kohda D, Nakakita SI, Hiramatsu H, Suzuki Y, Nakayama T, Terada T, Shimizu K, Shimizu N, Shiroishi M, Yanagi Y, Hashiguchi T. 2016. Trisaccharide containing alpha2,3-linked sialic acid is a receptor for mumps virus. Proc Natl Acad Sci U S A 113:11579–11584. https://doi.org/10.1073/pnas.1608383113.
7. Hosaka Y, Kuroda K, Ikeura A, Iwamoto T, Suzuki Y. 1998. Binding of influenza and paramyxoviruses to group B *Streptococcus* with the terminal sialyl-galactose linkage. J Electron Microsc (Tokyo) 47:169–174. https://doi.org/10.1093/oxfordjournals.jmicro.a023574.
8. Lamb RA. 1993. Paramyxovirus fusion: a hypothesis for changes. Virology 197:1–11. https://doi.org/10.1006/viro.1993.1561.
9. Wolinsky JS, Stroop WG. 1978. Virulence and persistence of three prototype strains of mumps virus in newborn hamsters. Arch Virol 57:355–359. https://doi.org/10.1007/BF01320075.
10. McCarthy M, Johnson RT. 1980. A comparison of the structural polypeptides of five strains of mumps virus. J Gen Virol 46:15–27. https://doi.org/10.1099/0022-1317-46-1-15.
11. Lamb RA, Paterson RG, Jardetzky TS. 2006. Paramyxovirus membrane fusion: lessons from the F and HN atomic structures. Virology 344:30–37. https://doi.org/10.1016/j.virol.2005.09.007.
12. Waxham MN, Server AC, Goodman HM, Wolinsky JS. 1987. Cloning and sequencing of the mumps virus fusion protein gene. Virology 159:381–388. https://doi.org/10.1016/0042-6822(87)90477-6.
13. Seidah NG, Day R, Marcinkiewicz M, Chretien M. 1998. Precursor convertases: an evolutionary ancient, cell-specific, combinatorial mechanism yielding diverse bioactive peptides and proteins. Ann N Y Acad Sci 839:9–24. https://doi.org/10.1111/j.1749-6632.1998.tb10727.x.
14. Walker JA, Molloy SS, Thomas G, Sakaguchi T, Yoshida T, Chambers TM, Kawaoka Y. 1994. Sequence specificity of furin, a proprotein-processing endoprotease, for the hemagglutinin of a virulent avian influenza virus. J Virol 68:1213–1218. https://doi.org/10.1128/JVI.68.2.1213-1218.1994.
15. Molloy SS, Bresnahan PA, Leppla SH, Klimpel KR, Thomas G. 1992. Human furin is a calcium-dependent serine endoprotease that recognizes the sequence Arg-X-X-Arg and efficiently cleaves anthrax toxin protective antigen. J Biol Chem 267:16396–16402.
16. Tian S, Huajun W, Wu J. 2012. Computational prediction of furin cleavage sites by a hybrid method and understanding mechanism underlying diseases. Sci Rep 2:261. https://doi.org/10.1038/srep00261.
17. Tian S, Huang Q, Fang Y, Wu J. 2011. FurinDB: a database of 20-residue furin cleavage site motifs, substrates and their associated drugs. Int J Mol Sci 12:1060–1065. https://doi.org/10.3390/ijms12021060.
18. Smith EC, Popa A, Chang A, Masante C, Dutch RE. 2009. Viral entry mechanisms: the increasing diversity of paramyxovirus entry. FEBS J 276:7217–7227. https://doi.org/10.1111/j.1742-4658.2009.07401.x.
19. Tanabayashi K, Takeuchi K, Okazaki K, Hishiyama M, Yamada A. 1992. Expression of mumps virus glycoproteins in mammalian cells from cloned cDNAs: both F and HN proteins are required for cell fusion. Virology 187:801–804. https://doi.org/10.1016/0042-6822(92)90482-5.
20. Merz DC, Wolinsky JS. 1981. Biochemical features of mumps virus neuraminidases and their relationship with pathogenicity. Virology 114:218–227. https://doi.org/10.1016/0042-6822(81)90267-1.
21. Merz DC, Server AC, Waxham MN, Wolinsky JS. 1983. Biosynthesis of mumps virus F glycoprotein: non-fusing strains efficiently cleave the F glycoprotein precursor. J Gen Virol 64 (Pt 7):1457–1467. https://doi.org/10.1099/0022-1317-64-7-1457.
22. Elango N, Varsanyi TM, Kovamees J, Norrby E. 1989. The mumps virus fusion protein mRNA sequence and homology among the paramyxoviridae proteins. J Gen Virol 70:801–807. https://doi.org/10.1099/0022-1317-70-4-801.
23. Malik T, Wolbert C, Mauldin J, Sauder C, Carbone KM, Rubin SA. 2007. Functional consequences of attenuating mutations in the haemagglutinin neuraminidase, fusion and polymerase proteins of a wild-type mumps virus strain. J Gen Virol 88:2533–2541. https://doi.org/10.1099/vir.0.82935-0.
24. Malik T, Sauder C, Wolbert C, Zhang C, Carbone KM, Rubin S. 2007. A single nucleotide change in the mumps virus F gene affects virus fusogenicity in vitro and virulence *in vivo*. J Neurovirol 13:513–521. https://doi.org/10.1080/13550280701658382.
25. Yoshida N, Nakayama T. 2010. Leucine at position 383 of fusion protein is responsible for fusogenicity of wild-type mumps virus in B95a cells. Intervirology 53:193–202. https://doi.org/10.1159/000299061.
26. Tanabayashi K, Takeuchi K, Okazaki K, Hishiyama M, Yamada A. 1993. Identification of an amino acid that defines the fusogenicity of mumps virus. J Virol 67:2928–2931. https://doi.org/10.1128/JVI.67.5.2928-2931.1993.
27. Kruger N, Hoffmann M, Drexler JF, Muller MA, Corman VM, Sauder C, Rubin S, He B, Orvell C, Drosten C, Herrler G. 2015. Functional properties and genetic relatedness of the fusion and hemagglutinin-neuraminidase proteins of a mumps virus-like bat virus. J Virol 89:4539–4548. https://doi.org/10.1128/JVI.03693-14.
28. Kruger N, Sauder C, Huttl S, Papies J, Voigt K, Herrler G, Hardes K, Steinmetzer T, Orvell C, Drexler JF, Drosten C, Rubin S, Muller MA, Hoffmann M. 2018. Entry, replication, immune evasion, and neurotoxicity of synthetically engineered bat-borne mumps virus. Cell Rep 25:312.e7–320.e7. https://doi.org/10.1016/j.celrep.2018.09.018.
29. Ozkutlu S, Soylemezoglu O, Calikoglu AS, Kale G, Karaaslan E. 1989. Fatal mumps myocarditis. Jpn Heart J 30:109–114. https://doi.org/10.1536/ihj.30.109.
30. Falk WA, Buchan K, Dow M, Garson JZ, Hill E, Nosal M, Tarrant M, Westbury RC, White FM. 1989. The epidemiology of mumps in southern Alberta 1980-1982. Am J Epidemiol 130:736–749. https://doi.org/10.1093/oxfordjournals.aje.a115395.
31. Bang H, Bang J. 1943. Involvement of the central nervous system in mumps. Acta Medica Scandinavica 113:487–505. https://doi.org/10.1111/j.0954-6820.1943.tb09179.x.
32. Brown J, Kirkland H, Hein G. 1948. Central nervous system involvement during mumps. Am J Med Sci 215:434–441. https://doi.org/10.1097/00000441-194804000-00012.
33. Love A, Rydbeck R, Ljungdahl A, Kristensson K, Norrby E. 1986. Selection of mutants of mumps virus with altered structure and pathogenicity by passage *in vivo*. Microb Pathog 1:149–158. https://doi.org/10.1016/0882-4010(86)90017-3.
34. Lemon K, Rima BK, McQuaid S, Allen IV, Duprex WP. 2007. The F gene of rodent brain-adapted mumps virus is a major determinant of neurovirulence. J Virol 81:8293–8302. https://doi.org/10.1128/JVI.00266-07.
35. Merz DC, Wolinsky JS. 1983. Conversion of nonfusing mumps virus infections to fusing infections by selective proteolysis of the HN glycoprotein. Virology 131:328–340. https://doi.org/10.1016/0042-6822(83)90501-9.
36. Tian S. 2009. A 20 residues motif delineates the furin cleavage site and its physical properties may influence viral fusion. Biochem Insights 2:BCI.S2049–20. https://doi.org/10.4137/BCI.S2049.
37. McCarthy M, Jubelt B, Fay DB, Johnson RT. 1980. Comparative studies of five strains of mumps virus *in vitro* and in neonatal hamsters: evaluation of growth, cytopathogenicity, and neurovirulence. J Med Virol 5:1–15. https://doi.org/10.1002/jmv.1890050102.
38. Cizman M, Mozetic M, Radescek-Rakar R, Pleterski-Rigler D, Susec-Michieli M. 1989. Aseptic meningitis after vaccination against measles and mumps. Pediatr Infect Dis J 8:302–308.
39. Andzhaparidze OG, Boriskin Yu S, Bogomolova NN, Drynov ID. 1982. Mumps virus-persistently infected cell cultures release defective interfering virus particles. J Gen Virol 63:499–503. https://doi.org/10.1099/0022-1317-63-2-499.
40. Amexis G, Rubin S, Chatterjee N, Carbone K, Chumakov K. 2003. Identification of a new genotype H wild-type mumps virus strain and its

molecular relatedness to other virulent and attenuated strains. J Med Virol 70:284–286. https://doi.org/10.1002/jmv.10392.
41. Dahms SO, Hardes K, Steinmetzer T, Than ME. 2018. X-ray structures of the proprotein convertase furin bound with substrate analogue inhibitors reveal substrate specificity determinants beyond the S4 pocket. Biochemistry 57:925–934. https://doi.org/10.1021/acs.biochem.7b01124.
42. Liu Y, Xu Y, Lou Z, Zhu J, Hu X, Gao GF, Qiu B, Rao Z, Tien P. 2006. Structural characterization of mumps virus fusion protein core. Biochem Biophys Res Commun 348:916–922. https://doi.org/10.1016/j.bbrc.2006.07.168.
43. Liu Y, Xu Y, Zhu J, Qiu B, Rao Z, Gao GF, Tien P. 2005. Crystallization and preliminary X-ray diffraction analysis of central structure domains from mumps virus F protein. Acta Crystallogr Sect F Struct Biol Cryst Commun 61:855–857. https://doi.org/10.1107/S1744309105025789.
44. Molloy SS, Anderson ED, Jean F, Thomas G. 1999. Bi-cycling the furin pathway: from TGN localization to pathogen activation and embryogenesis. Trends Cell Biol 9:28–35. https://doi.org/10.1016/s0962-8924(98)01382-8.
45. Liu G, Thomas L, Warren RA, Enns CA, Cunningham CC, Hartwig JH, Thomas G. 1997. Cytoskeletal protein ABP-280 directs the intracellular trafficking of furin and modulates proprotein processing in the endocytic pathway. J Cell Biol 139:1719–1733. https://doi.org/10.1083/jcb.139.7.1719.
46. Klimpel KR, Molloy SS, Thomas G, Leppla SH. 1992. Anthrax toxin protective antigen is activated by a cell surface protease with the sequence specificity and catalytic properties of furin. Proc Natl Acad Sci U S A 89:10277–10281. https://doi.org/10.1073/pnas.89.21.10277.
47. Abrami L, Fivaz M, Decroly E, Seidah NG, Jean F, Thomas G, Leppla SH, Buckley JT, van der Goot FG. 1998. The pore-forming toxin proaerolysin is activated by furin. J Biol Chem 273:32656–32661. https://doi.org/10.1074/jbc.273.49.32656.
48. Thomas G. 2002. Furin at the cutting edge: from protein traffic to embryogenesis and disease. Nat Rev Mol Cell Biol 3:753–766. https://doi.org/10.1038/nrm934.
49. Rodenhuis-Zybert IA, van der Schaar HM, da Silva Voorham JM, van der Ende-Metselaar H, Lei HY, Wilschut J, Smit JM. 2010. Immature dengue virus: a veiled pathogen? PLoS Pathog 6:e1000718. https://doi.org/10.1371/journal.ppat.1000718.
50. Day PM, Schiller JT. 2009. The role of furin in papillomavirus infection. Future Microbiol 4:1255–1262. https://doi.org/10.2217/fmb.09.86.
51. Klenk HD, Garten W. 1994. Host cell proteases controlling virus pathogenicity. Trends Microbiol 2:39–43. https://doi.org/10.1016/0966-842x(94)90123-6.
52. de Haan CA, Stadler K, Godeke GJ, Bosch BJ, Rottier PJ. 2004. Cleavage inhibition of the murine coronavirus spike protein by a furin-like enzyme affects cell-cell but not virus-cell fusion. J Virol 78:6048–6054. https://doi.org/10.1128/JVI.78.11.6048-6054.2004.
53. Henis YI, Herman-Barhom Y, Aroeti B, Gutman O. 1989. Lateral mobility of both envelope proteins (F and HN) of Sendai virus in the cell membrane is essential for cell-cell fusion. J Biol Chem 264:17119–17125.
54. Konopka K, Pretzer E, Duzgunes N. 1995. Differential effects of a hydrophobic tripeptide on human immunodeficiency virus type 1 (HIV-1)-induced syncytium formation and viral infectivity. Biochem Biophys Res Commun 208:75–81. https://doi.org/10.1006/bbrc.1995.1307.
55. Konopka K, Pretzer E, Celada F, Duzgunes N. 1995. A monoclonal antibody to the gp120-CD4 complex has differential effect on HIV-induced syncytium formation and viral infectivity. J Gen Virol 76:669–679. https://doi.org/10.1099/0022-1317-76-3-669.
56. Pleskoff O, Seman M, Alizon M. 1995. Amphotericin B derivative blocks human immunodeficiency virus type 1 entry after CD4 binding: effect on virus-cell fusion but not on cell-cell fusion. J Virol 69:570–574. https://doi.org/10.1128/JVI.69.1.570-574.1995.
57. Hernandez LD, Hoffman LR, Wolfsberg TG, White JM. 1996. Virus-cell and cell-cell fusion. Annu Rev Cell Dev Biol 12:627–661. https://doi.org/10.1146/annurev.cellbio.12.1.627.
58. Jolly C, Booth NJ, Neil SJ. 2010. Cell-cell spread of human immunodeficiency virus type 1 overcomes tetherin/BST-2-mediated restriction in T cells. J Virol 84:12185–12199. https://doi.org/10.1128/JVI.01447-10.
59. Casartelli N, Sourisseau M, Feldmann J, Guivel-Benhassine F, Mallet A, Marcelin AG, Guatelli J, Schwartz O. 2010. Tetherin restricts productive HIV-1 cell-to-cell transmission. PLoS Pathog 6:e1000955. https://doi.org/10.1371/journal.ppat.1000955.
60. Richardson MW, Carroll RG, Stremlau M, Korokhov N, Humeau LM, Silvestri G, Sodroski J, Riley JL. 2008. Mode of transmission affects the sensitivity of human immunodeficiency virus type 1 to restriction by rhesus TRIM5alpha. J Virol 82:11117–11128. https://doi.org/10.1128/JVI.01046-08.
61. Mothes W, Sherer NM, Jin J, Zhong P. 2010. Virus cell-to-cell transmission. J Virol 84:8360–8368. https://doi.org/10.1128/JVI.00443-10.
62. Sattentau Q. 2008. Avoiding the void: cell-to-cell spread of human viruses. Nat Rev Microbiol 6:815–826. https://doi.org/10.1038/nrmicro1972.
63. Buchholz UJ, Finke S, Conzelmann KK. 1999. Generation of bovine respiratory syncytial virus (BRSV) from cDNA: BRSV NS2 is not essential for virus replication in tissue culture, and the human RSV leader region acts as a functional BRSV genome promoter. J Virol 73:251–259. https://doi.org/10.1128/JVI.73.1.251-259.1999.
64. Sauder CJ, Vandenburgh KM, Iskow RC, Malik T, Carbone KM, Rubin SA. 2006. Changes in mumps virus neurovirulence phenotype associated with quasispecies heterogeneity. Virology 350:48–57. https://doi.org/10.1016/j.virol.2006.01.035.
65. Knoppova M, Phensaijai M, Vesely M, Zemanova M, Nesvera J, Patek M. 2007. Plasmid vectors for testing *in vivo* promoter activities in *Corynebacterium glutamicum* and *Rhodococcus erythropolis*. Curr Microbiol 55:234–239. https://doi.org/10.1007/s00284-007-0106-1.
66. Kruger N, Sauder C, Hoffmann M, Orvell C, Drexler JF, Rubin S, Herrler G. 2016. Recombinant mumps viruses expressing the batMuV fusion glycoprotein are highly fusion active and neurovirulent. J Gen Virol 97:2837–2848. https://doi.org/10.1099/jgv.0.000596.
67. Berger Rentsch M, Zimmer G. 2011. A vesicular stomatitis virus replicon-based bioassay for the rapid and sensitive determination of multi-species type I interferon. PLoS One 6:e25858. https://doi.org/10.1371/journal.pone.0025858.
68. Hoffmann M, Müller MA, Drexler JF, Glende J, Erdt M, Gützkow T, Losemann C, Binger T, Deng H, Schwegmann-Weßels C, Esser K-H, Drosten C, Herrler G. 2013. Differential sensitivity of bat cells to infection by enveloped RNA viruses: coronaviruses, paramyxoviruses, filoviruses, and influenza viruses. PLoS One 8:e72942. https://doi.org/10.1371/journal.pone.0072942.
69. Kuhl A, Hoffmann M, Muller MA, Munster VJ, Gnirss K, Kiene M, Tsegaye TS, Behrens G, Herrler G, Feldmann H, Drosten C, Pohlmann S. 2011. Comparative analysis of Ebola virus glycoprotein interactions with human and bat cells. J Infect Dis 204 (Suppl 3):S840–S849. https://doi.org/10.1093/infdis/jir306.
70. Lefrancois L, Lyles DS. 1982. The interaction of antibody with the major surface glycoprotein of vesicular stomatitis virus. I. Analysis of neutralizing epitopes with monoclonal antibodies. Virology 121:157–167. https://doi.org/10.1016/0042-6822(82)90125-8.
71. Orvell C, Alsheikhly AR, Kalantari M, Johansson B. 1997. Characterization of genotype-specific epitopes of the HN protein of mumps virus. J Gen Virol 78:3187–3193. https://doi.org/10.1099/0022-1317-78-12-3187.
72. Hardes K, Becker GL, Lu Y, Dahms SO, Kohler S, Beyer W, Sandvig K, Yamamoto H, Lindberg I, Walz L, von Messling V, Than ME, Garten W, Steinmetzer T. 2015. Novel furin inhibitors with potent anti-infectious activity. ChemMedChem 10:1218–1231. https://doi.org/10.1002/cmdc.201500103.